



## SHEAR RESISTANCE OF RC INTERIOR ECCENTRIC BEAM-COLUMN JOINTS

Yasuaki GOTO<sup>1</sup>, Osamu JOH<sup>2</sup>

### SUMMARY

Experimental study was carried out to clarify the influence of eccentricity on the shear strength and failure mechanism of reinforced concrete interior beam-column joints. Four half-scale, cross-shaped specimens were tested to investigate the relationship of eccentricity and strength reduction. Test results show that the larger the eccentric distance, the smaller the joint shear strength. Continuous analytical study by three-dimensional inelastic finite element analysis was carried out to examine precisely the shear failure mechanism of these joints. The analytical results show that the concentration of the shear stress of joint concrete is on the eccentric side and in the region of concrete failure.

### INTRODUCTION

The beam-column joints in many reinforced concrete (RC) buildings suffered damage during the disastrous Hyogoken-Nanbu earthquake in 1995. In 1999, design requirements for beam-column joints were enacted in the AIJ (Architectural Institute of Japan) standard for RC structures [1], which is a well-known design guide in Japan. Researchers have investigated the cause of failure of these damaged buildings. They found that almost all damaged frames showed eccentricity between the beam and column, and the joint shear strengths calculated according to the AIJ RC standard were enough larger than the flexural strength of adjacent beams to cause flexural failure at the beam ends [2]. Therefore, they concluded the reduction of joint shear strength might occur in the actual buildings due to the eccentricity between the beam and column. Because there has not been much research on eccentric beam-column joints, the influence of eccentricity on joint shear strength and frame deformability has not been clarified [3]. In some design codes that include the AIJ RC standard, the influence of eccentricity on joint shear strength uses the effective joint width [4][5]. For example, the effective joint width according to the AIJ RC standard is calculated as the beam width plus the minimum value of half the distance between the column face and beam face, or a quarter of the joint depth on both sides. The joint shear strength is calculated as the product of the effective joint area (defined by the effective width and column depth) and the standard strength that depends on the joint concrete strength, configuration and confinement condition. In addition, joint reinforcement does not effect joint shear strength, but it is does effect the confinement of the joint core concrete, which results in ductile behavior of the frame.

The failure mode of the beam-column sub-assemblage is defined as follows: when the joint shear

<sup>1</sup> Associate Professor, Hokkaido University, Sapporo, Japan. Email: gotsu@eng.hokudai.ac.jp

<sup>2</sup> Professor, Hokkaido University, Sapporo, Japan. Email: joh@eng.hokudai.ac.jp

strength is large enough, adjacent beams will yield and beam flexural failure will occur (B-type). But in the case that the joint shear strength is not large enough against the beam flexural strength, joint shear failure occurs with a large displacement after beam yielding (BJ-type). If large amounts of beam bars are provided, the beam flexural strength becomes so large that joint shear failure will occur before beam yielding (J-type). Besides these failure types, flexural and shear failure of both beam and column members is expected, and also bond failure will be observed in such cases as poor bond conditions, which occurs when using large-diameter bars as longitudinal reinforcements [6].

The RC frame is designed according to the weak-beam, strong-column concept, so that large energy dissipation is expected, which leads to the preferable behavior of structures. It is necessary to establish the evaluation of not only joint shear strength but also the deformability of several types of frame configurations in structural design. This study presents test results on the performance of eccentric beam-column sub-assemblages subjected to vertical gravity and lateral earthquake loading, and the analytical results of the shear failure mechanism of joints.

## EXPERIMENTAL PROGRAM

## Experimental work

### Specimens

All specimens were cross-shaped in order to focus on the interior beam-column sub-assemblages. Specimens had neither transverse beams nor floor slabs (plane frames). The size of each beam and column was the same for all specimens (beam section 200 x 350 mm, length 3,000 mm; column section 450 x 300 mm, height 1,750 mm). The differences in eccentric distance between the beam center and column center of the specimens was set as 0, 60 or 125 mm, which gives eccentricity ratios of 0, 0.12 and 0.25, respectively. In addition, the joint reinforcement ratios were set as 0.25% (use letter "M") and 0.53% (use letter "U") volumetric ratios. For the specimen names, the second letter and first number after the hyphen represent the joint reinforcement ratio and eccentric distance, respectively. Table 1 shows the properties of all specimens.

The joint shear strength of all specimens was calculated according to the AIJ Standard. All specimens were designed not to show shear failure of the beam or column prior to expected failure. In order to clarify the influence of eccentricity on the joint shear strength, all specimens were designed to fail because of joint shear failure. Therefore, a large number of beam bars were provided in order to generate large input to each joint. Figure 1 illustrates in detail the reinforcement of the specimens. In the specimens, a steel cover plate was attached to the beam concrete at the beam ends in order to prevent the concrete from being crushed due to compressive force. The first letter of the specimen names indicates the joint shear input at beam yielding, which is defined by the product of the beam bar area and its tensile strength.

Table 1. Specimen list

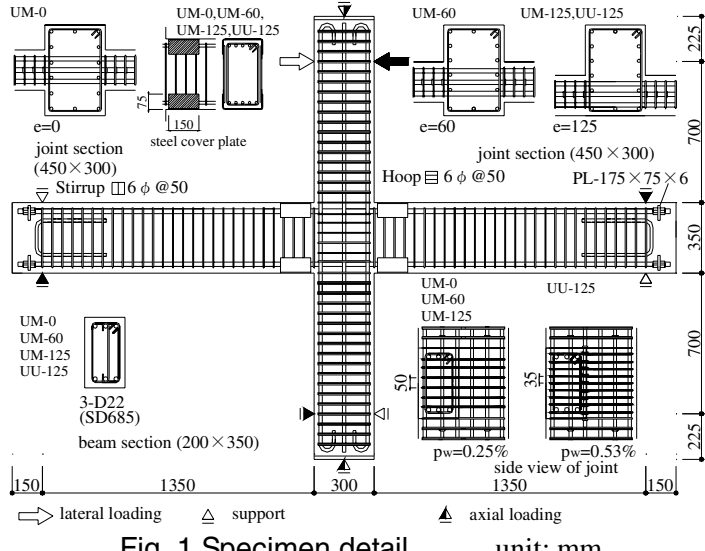


Fig. 1 Specimen detail      unit: mm

### Materials

The design compressive strength of the concrete was 24 MPa. The concrete consisted of crushed stone having a maximum size of 13 mm. Table 2 summarizes the actual compressive strengths of the concrete on test day. Table 3 shows the mechanical properties of the flexural reinforcing bars and joint reinforcement. The stress-strain relationship of each bar was obtained by attaching a strain gage during the material testing, and the measured strain in this relationship was used to calculate the stress generated in the reinforcement.

Table 2. Concrete properties

Specimen	$\sigma_B$ (MPa)	$\varepsilon_{max}$ ( $\mu$ )	$\sigma_t$ (MPa)	$E_{1/3}$ (GPa)
UM-0	24.0	2480	1.88	21.0
UM-60	24.6	2590	2.46	22.9
UM-125	25.2	2640	2.34	22.9
UU-125	25.4	2530	2.11	23.5

Table 3. Reinforcement properties

Classification	$\sigma_y$ (MPa)	$\varepsilon_y$ ( $\mu$ )	$\sigma_{max}$ (MPa)	$E_s$ (GPa)	Elongation (%)
6φ SR295	355	1780	432	200	20.4
D6 SD345	495	2610	531	190	15.0
D16 SD345	384	2325	572	-	21.7
D22 SD685	697	5740	979	186	10.0

### Loading

Figure 2 shows the loading setup. Specimens were tested in the upright position. The column was linked to a reaction wall by channel steel at the bottom and a hydraulic actuator at the top. The end of each beam (reflection point) was linked to the reaction floor by a pinned-end vertical support. Axial force was generated by a hydraulic jack at the column bottom and an actuator at the column top. Specimens were also supported perpendicular to the loading plane (i.e., perpendicular to the paper). The torsion generated due to eccentricity was restrained by H-shaped steel mounted at the column top and bottom.

First, a constant column axial force was applied up to 1/6 of the concrete compressive strength in stress, and then a lateral displacement was applied to the column top statically. Reversal displacements of 1/500, 1/200, 1/100 (2), 1/70 (2), 1/50 (2), 1/35 and 1/20 in the story drift angle were applied cyclically. The numbers in parentheses indicate the number of repetitions of the same displacement.

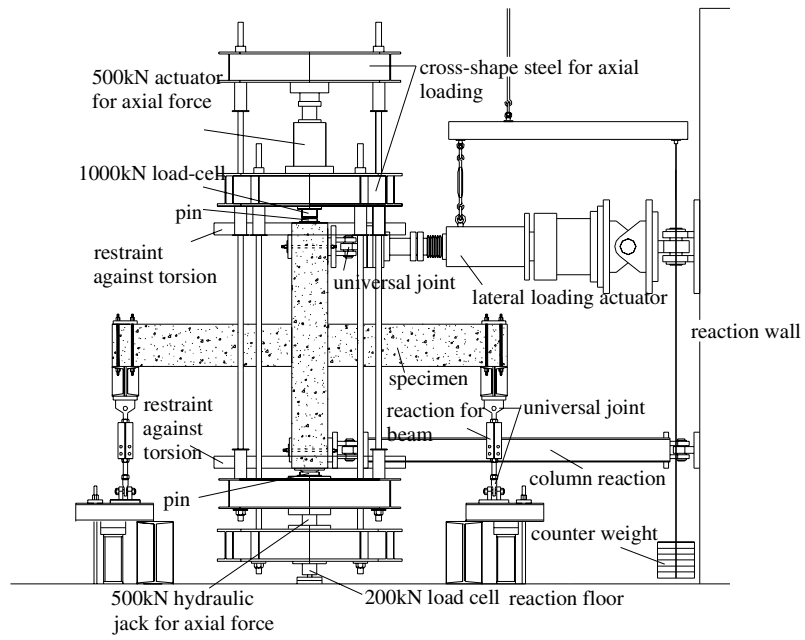


Fig. 2 Loading setup

## Discussion of test results

### *Crack pattern*

Figure 3 shows the typical joint cracking pattern that was observed after testing. Severe joint shear cracking was observed on the flush side, but only a small crack appeared on the offset side. Beam bar yielding was not observed during testing. Specimen UM-0, in which the eccentric distance was equal to 0,

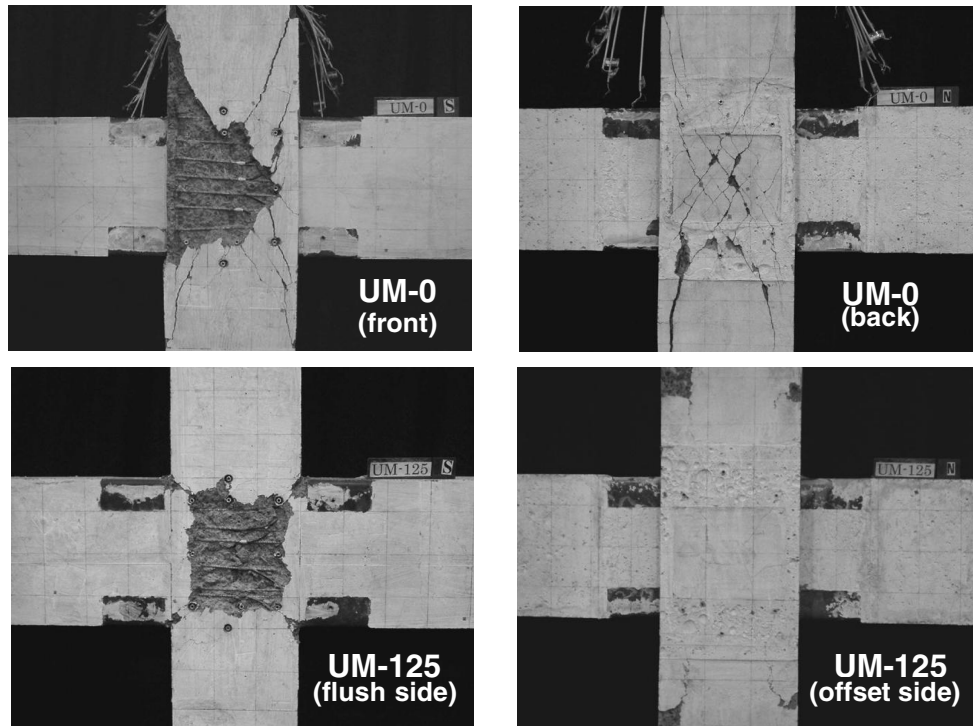


Fig. 3 Specimen appearance after test  
(black pieces in beam-end are steel covers)

had severe joint shear cracking on both sides. The joint cover concrete spalled out when the story drift angle became larger than 0.03 and severe cracking was observed. Torsional cracking was also observed at the column faces of the eccentric specimens where the beams were connected.

#### *Story shear vs. story drift angle*

Figure 4 shows the envelope curves of story shear vs. story drift angle for all specimens. The initial stiffness of each specimen was similar, but the degradation became obvious after concrete compressive fracture was observed in the joint. This figure also indicates that the maximum strength primarily depends on the eccentric distance.

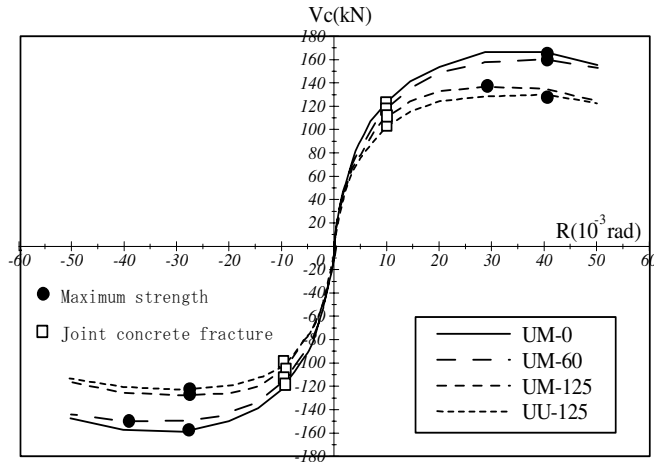


Fig. 4 Story shear vs. story drift angle

#### *Ultimate strength*

Table 4 shows the test results for the column shear of all specimens and compares the beam flexural strength and joint shear strength calculated by the proposed equations. The failure mode of all specimens was defined as joint shear failure (J-type), because no yielding of the beam bar was observed, but severe joint concrete fracture was observed. Figure 5 shows the relationship between maximum strength and eccentricity ratio. This figure indicates that the tendency for the shear strength becomes smaller as the eccentricity ratio increases. Therefore, the influence of eccentricity on strength reduction should be examined.

The calculated beam flexural strength (cal1 in Table 4) is larger than the experimental results for all specimens, because beam yielding did not occur.

The two proposed equations shown in the footnote of Table 4 are used to calculate the joint shear strength. These two equations differ in their consideration of eccentricity. In Table 4, cal2 is calculated by equation 2, using the effective joint width defined in Figure 6, and cal3 is calculated by equation 3, with direct consideration of the torsional moment. The value of the joint shear strength\_calculated using either the cal2 or cal3 equation underestimates the test results, while the ratio of the calculated to observed strength decreases as the eccentric distance increases. This means that the estimation of the factor of safety for joint shear failure changes according to the eccentric distance. The definition of effective joint width was also examined in order to improve the estimation. For the case in which the beam is connected at the center of the column, the effective joint width is smaller than the width of the joint core concrete. If large eccentricity exists between the beam and the column, the proposed effective width includes the joint cover concrete, which was no longer effective at the ultimate stage of the test due to having been spalled out. Therefore, the effective joint width should be modified to exclude the thickness of the cover concrete. The calculated values using the modified width (cal4) also underestimate the test results, but the ratio is almost constant despite the change in eccentric distance.

Table 4. Test results

Specimen	$\text{exp}V_c$ (kN)	Beam flexural		Joint shear						Failure mode	
		Equation 2		Equation 3		Eq. 2 (modified width)					
		$\text{cal}_1 V_c$	exp/cal	$\text{cal}_2 V_c$	exp/cal	$\text{cal}_3 V_c$	exp/cal	$\text{cal}_4 V_c$	exp/cal		
UM-0	166.5	272.0	0.61	125.9	1.32	-	-	125.9	1.32	J	
UM-60	160.0	272.0	0.59	121.4	1.32	114.2	1.40	121.0	1.32	J	
UM-125	137.0	272.0	0.50	110.2	1.24	91.8	1.49	97.0	1.41	J	
UU-125	130.0	272.0	0.48	110.8	1.17	98.2	1.32	97.5	1.33	J	

cal1 :  $M_u = 0.9 \cdot a_t \cdot \sigma_y \cdot d_b$  (1) cal2 :  $V_{ju} = \kappa_2 \cdot \phi \cdot F_j \cdot b_{ju} \cdot D_c$  (2)

cal3 :  $V_{ju} = \beta_{jt} \cdot \text{cal}_2 V_{ju}$  (3)  $\beta_{jt} = \left\{ 1 + \left( e \cdot \text{cal}_2 V_{ju} / T_{ju} \right)^2 \right\}^{-0.5}$ ,  $T_{ju} = (0.8\sqrt{\sigma_B} + 0.45 p_w \cdot \sigma_{wy}) \cdot b_c^2 \cdot D_c$

where, unit: N, mm, MPa

$M_u$ : beam flexural strength  $V_{ju}$ : joint shear strength  $T_{ju}$ : torsional strength

$a_t$ : bar area  $\sigma_y$ : yield strength  $d_b$ : beam effective depth  $\kappa_2$ : 1.0 (configuration factor)  $b_{ju}$ : effective joint width

$\phi$ : 0.85 (confinement by transverse beams)  $F_j$ :  $0.8 \times \sigma_B^{0.7}$  (standard strength)  $D_c$ : column depth  $b_c$ : column width

$\sigma_B$ : concrete compressive strength  $p_w$ : joint reinforcement ratio  $\sigma_{wy}$ : yield strength of joint reinforcement

$\text{exp}V_c$  (kN)

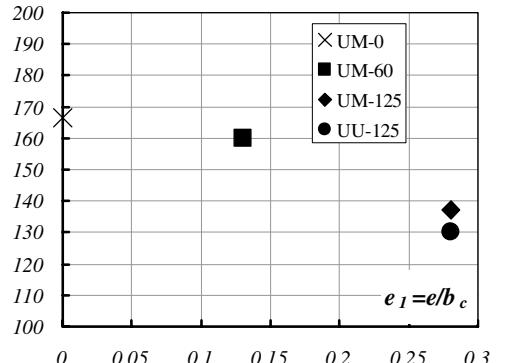


Fig.5 Relation of observed strength and eccentric distance

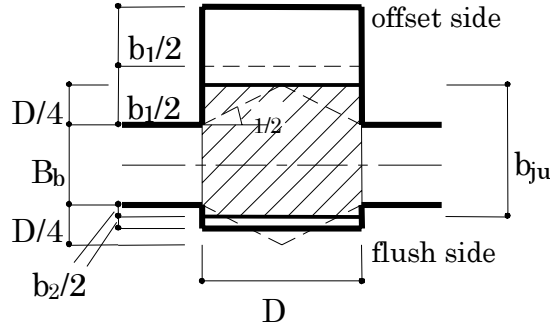


Fig. 6 Joint effective width (AIJ RC standard)

## ANALYTICAL PROGRAM

### Analytical method

#### Reference specimens

Three specimens of UM-0, UM-60 and UM-125 were selected as reference specimens for the finite element method (FEM) analytical program to examine the influence of eccentricity on the shear failure mechanism of an eccentric beam-column joint.

#### Analytical model

A three-dimensional analysis program was needed for the concentric joint when the widths of the column and beam were not the same, and more needed for the eccentric joint. This analysis was carried out using the DIANA (ver. 7.2) finite element program developed by TNO. The analytical model for each specimen is shown in Figure 7. In the analysis, incremental displacements were given to both beam ends under constant column axial force, whereas the column displacement was given in the experimental work, because no P-delta moment was generated with the axial loading system. Boundary conditions in the analysis were applied according to the experiment. The torsion-restraining steel at the column end was also modeled using beam elements, because pre-analysis showed that the presence of the fixed support greatly influenced the result in the eccentric joint. However, the fixed support was also applied in UM-0 of the concentric joint.

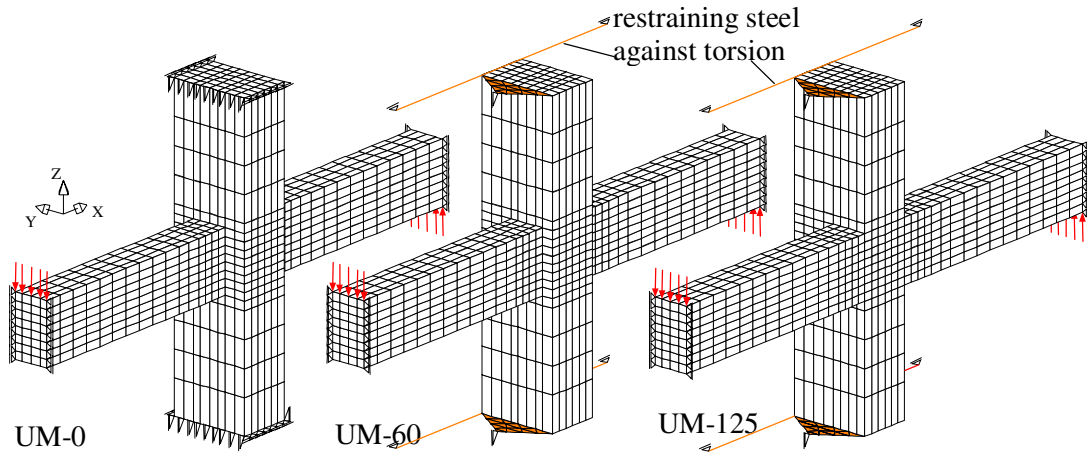


Fig. 7 Analytical model

#### *Material models*

##### (a) Concrete

Eight-node solid brick elements with four Gaussian points were assumed for the concrete. In the constitutive model of the concrete, an ascending compressive stress-strain relationship was represented by the CEB Model Code (1990)[7], and the failure was evaluated by the failure criterion of Drucker-Prager [8]. The post-peak behavior of the concrete at the beam end was modeled to not show stress relaxing because of the existence of the restraint steel cover, whereas the other concrete was modeled as the softening model shown in Figure 8, as defined by equation (4) based on the compressive fracture energy by Nakamura et al. [9]. The equivalent element length was defined as the diameter of the sphere with a volume equal to that of the concrete element. The smeared crack model was represented in the concrete element, where tension softening was considered according to the equation proposed by Hordijk [10].

$$G_{fc} = 8.8\sqrt{f_c} \quad (4)$$

where,

$G_{fc}$  : concrete compressive fracture energy (N/mm)

$f_c$  : concrete compressive strength (MPa)

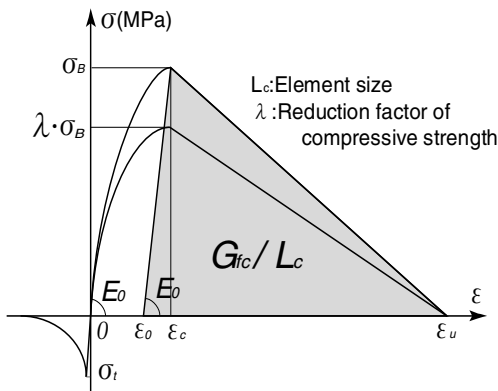


Fig. 8 Equivalent uni-axial stress-strain curve of concrete

### (b) Reinforcement

All reinforcement was assumed to be from two-node truss elements. The stress-strain relationship of these reinforcements was assumed to be bi-linear or tri-linear in accordance with the material test results.

### (c) Bond

The bond between the beam longitudinal reinforcement and concrete was expressed by line interface elements. Bond properties, including the stiffness and strength of bond stress vs. the slip relationship, depend on the condition around the reinforcement. The stress condition around the joint is considered to be that shown in Figure 9. The beam bars in the compressive region were subjected to clamping stress orthogonally by the compressive stress of the column bending, which causes larger stiffness and larger bond strength. The model for the bond stress vs. slip relationship, recommended by the CEB Model Code and shown in Figure 10, was adopted in this analysis; two types of conditions were applied for the consideration mentioned above, i.e. good condition or other condition in the bond. The bond properties are shown in Table 5. The bond for the other reinforcement of the column bar and shear reinforcement was assumed to be perfect (no slip).

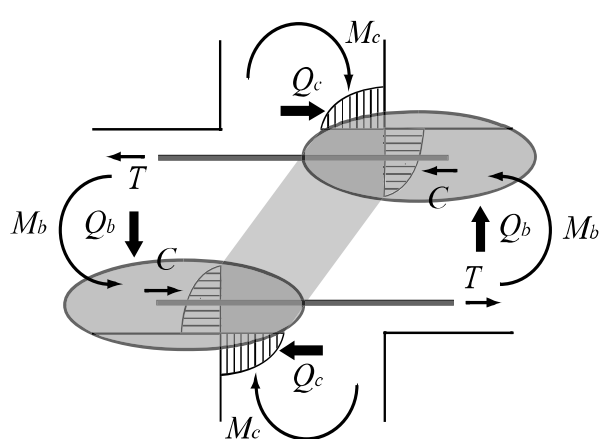


Fig. 9 Stress condition in joint

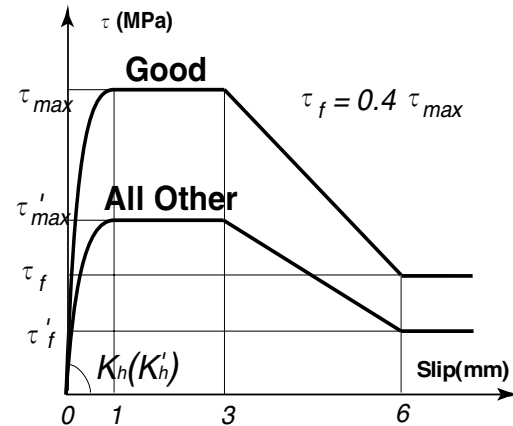


Fig. 10 Bond stress-slip relationship

Table 5. Bond specification

Specimen	UM-0		UM-60		UM-125	
Bond condition	Good	Other	Good	Other	Good	Other
$K_h$ (MPa/mm)	74.2	37.2	73.2	36.6	76.6	38.4
$\tau_{max}$ (MPa)	12.30	6.15	12.14	6.07	12.70	6.35

### Definition of the compressive failure of concrete element

The failure criterion of Drucker-Prager was adopted as the failure judgment in this analysis. To detect a failed concrete element, the three principal stresses calculated at each Gaussian point in the element were substituted into equation (5), then the element was identified as failed when the values of this equation for all Gaussian points within it were zero.

$$f(I_1, J_2) = \alpha \cdot I_1 + \sqrt{J_2} - k = 0 \quad (5)$$

where,

$$\alpha = \frac{2 \sin \phi}{\sqrt{3}(3 - \sin \phi)}, \quad k = \frac{6c \cdot \sin \phi}{\sqrt{3}(3 - \sin \phi)}$$

$I_1$ : first invariant of stresses

$J_2$ : second invariant of stresses

$\phi$ : angle of internal angle

$c$ : cohesion stress

### Reduction factor of joint concrete

Past experimental study has demonstrated that the concrete strut that is formed between shear cracks can help the resistance mechanism of RC members subjected to shear, but reduction of the concrete compressive strength occurs according to the increment of the cracking. Collins et al. [11] and Noguchi et al. [12] proposed an equation using the principal tensile strain of concrete to represent this characteristic. The research work in this paper could not consider this influence, so the following procedure was adopted. First, an analysis was carried out using the normal strength obtained by material testing, and the maximum tensile strain of the concrete elements at ultimate strength was obtained in each slice of block shown in Figure 11. Then, the reduction factor of each slice of block was calculated using Noguchi's equation (6), in which the maximum tensile strain of the block was substituted. Finally, the same analysis was carried out again using the reduction factor for joint concrete, which influenced the stiffness of the joint concrete. The reduction factor of each specimen is shown in Table 6.

$$\lambda = \frac{1}{0.27 + 0.96 \left( \frac{\varepsilon_{lu}}{\varepsilon_0} \right)^{0.167}} \quad (6)$$

where,

$\lambda$ : reduction factor for concrete compressive strength

$\varepsilon_{lu}$ : principal tensile strain of concrete

$\varepsilon_0$ : strain at maximum compressive strength

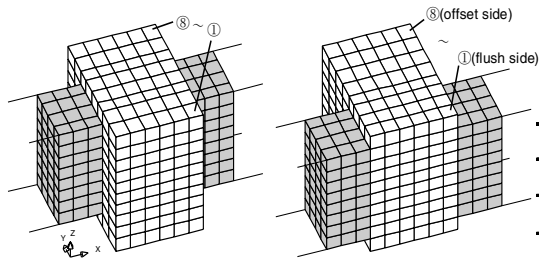


Table 6. Reduction factor  
of concrete compressive strength

Specimen	①	②	③	④	⑤	⑥	⑦	⑧
UM-0	0.59	0.61	0.60	0.59	0.59	0.60	0.61	0.59
UM-60	0.58	0.59	0.59	0.59	0.59	0.59	0.61	0.66
UM-125	0.56	0.58	0.60	0.61	0.61	0.62	0.67	0.78

Fig. 11 Location of joint concrete elements

### Analytical results and discussion

#### Story shear vs. story drift angle

The analytical results of all specimens were compared with the experimental results, as shown in Figure 12. The deterioration of stiffness in the analysis became smaller than the experimental result, which resulted in the larger ultimate strength. However, the strength reduction according to the increment of eccentric distance was obtained in the analytical results, and observed in the experimental results. UM-0 showed greater post-peak reduction of strength than did the eccentric joints. This is because the extension of the failure zone in the joint concrete was limited in the eccentric joint of UM-0, which will be detailed later. The failure mode of all specimens in the analysis was defined as joint shear (J-type), which coincides with the experimental results.

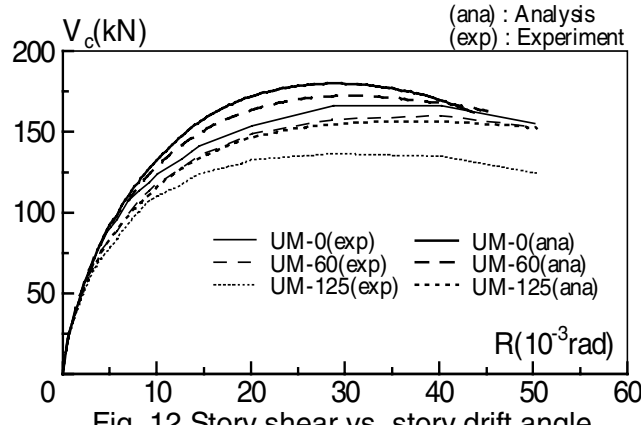


Fig. 12 Story shear vs. story drift angle

#### *Joint shear vs. joint shear distortion angle*

The analytical results on each flush side and offset side are shown in Figure 13. Joint shear is calculated from equation (7) in the experimental results on the assumption that the beam moment arm is 7/8 of the effective depth. On the other hand, the analytical value is obtained as the sum of the element shear located in the layer at the middle height of the joint, which is the integral of the shear stress obtained at the Gaussian points. The shear deformation of the analytical result is calculated from the displacement in the joint diagonal direction, which is the same procedure used in the experiment. The shear deformation angle on the flush side became larger with the increase of the eccentric distance. On the contrary, reverse joint deformation occurred on the offset side of UM-125, which was similar to the experimental result, and was caused by the torsional force that acted as a cancel shear on this side. However, the joint deformation reversed at the large displacement due to the increment of shear stress in the concrete element located on the offset side.

$$V_j = C_c + C_s + T_s - V_c = 2T - V_c \quad (7)$$

where,

$V_j$ : joint shear

$C_c$ : compressive force acting at concrete

$C_s$ : compressive force acting at beam bars

$T_s$ : tensile force at beam bars

$V_c$ : column shear

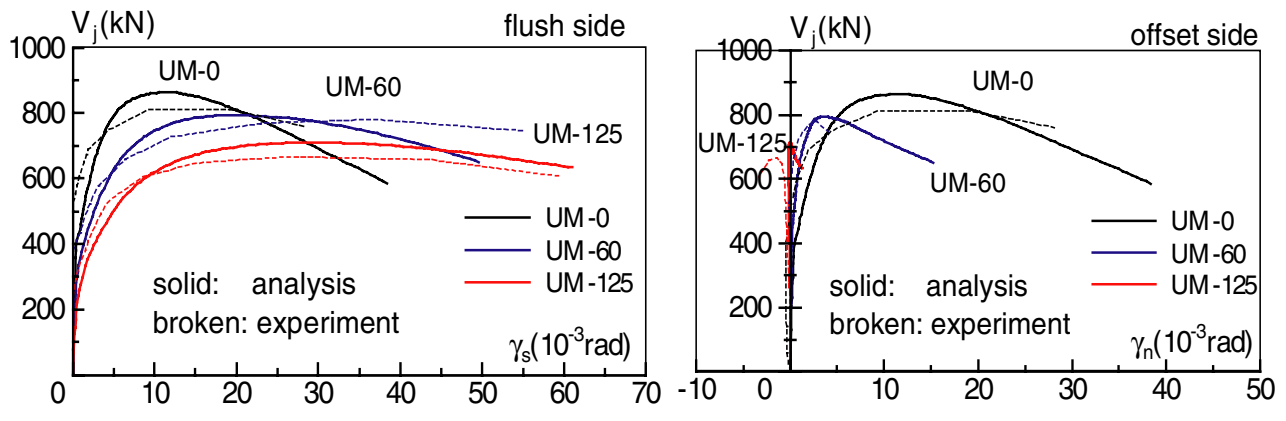


Fig. 13 Joint shear vs. joint shear distortion angle

### *Torsional moment vs. torsional deformation angle*

The analytical results of the eccentric joints are shown in Figure 14. The torsional moment was calculated as the product of the joint shear and eccentric distance, and the torsional displacement angle was calculated from the horizontal displacement of points that were located on the top and bottom of the joint on both the flush side and offset side. The analysis shows good agreement with the experiment.

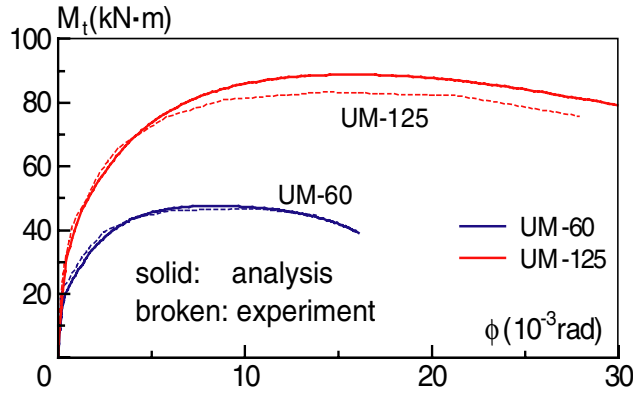


Fig. 14 Joint torsional moment vs. torsional deformation angle

### *Compressive stress distribution of joint concrete*

Figure 15 shows the distribution of compressive stress at the story drift angle of 1/100 radian and the maximum strength of two specimens, UM-0 and UM-125, in order to examine the influence of eccentricity on the stress distribution. Each row in Figure 15 represents slices of the block of elements. The region where the compressive stress became large is recognized approximately at the joint diagonal line, and so it is considered that a concrete compressive strut was formed. The concrete strut was distributed eccentrically to the beam-connected portions. After the ultimate stage, the compressive stress in the eccentric joint (UM-125) decreased due to failure on the flush side joint center and the extended strut towers to the opposite side, while the strut extended uniformly on both sides in the concentric joint (UM-0).

### *Shear stress distribution of joint concrete*

Figure 16 shows the shear stress distribution at the middle height of the joint in two specimens, UM-0 and UM-125. Symmetric distribution was observed in the concentric joint and the stress decreased in all areas after the ultimate stage. Eccentric distribution similar to the distribution of compressive stress was also observed in the eccentric joint, but the region where the shear stress increased shifted to the offset side after the ultimate stage while the stress decreased on the flush side simultaneously.

### *Failure of joint concrete*

In Figure 17, the hatched one indicates the failure of the joint concrete elements at the ultimate stage. Failure occurred in the elements colored in red, judging by the Drucker-Prager criterion. In the concentric joint, the failure zone distributed symmetrically to the joint face. However, failure was not observed on the offset side of the eccentric joint.

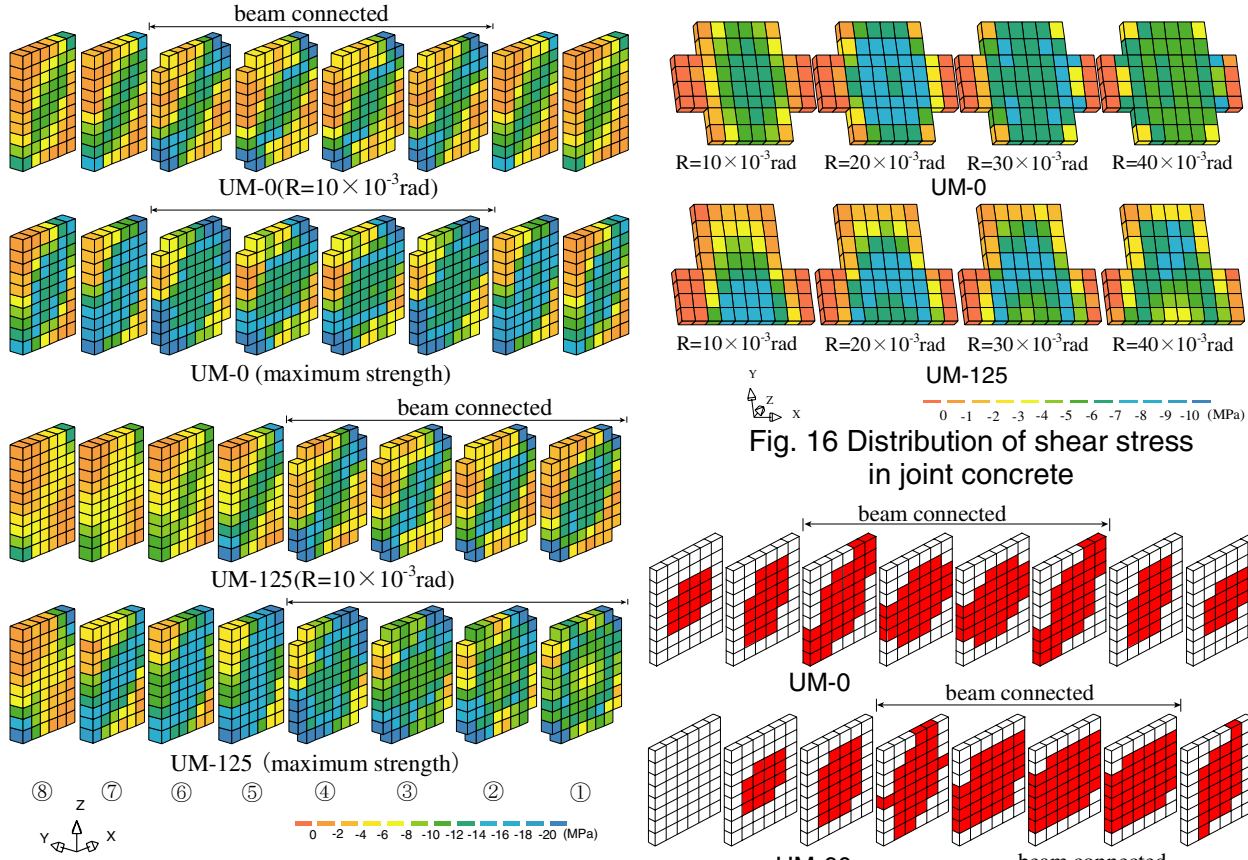


Fig. 15 Distribution of compressive stress in joint concrete

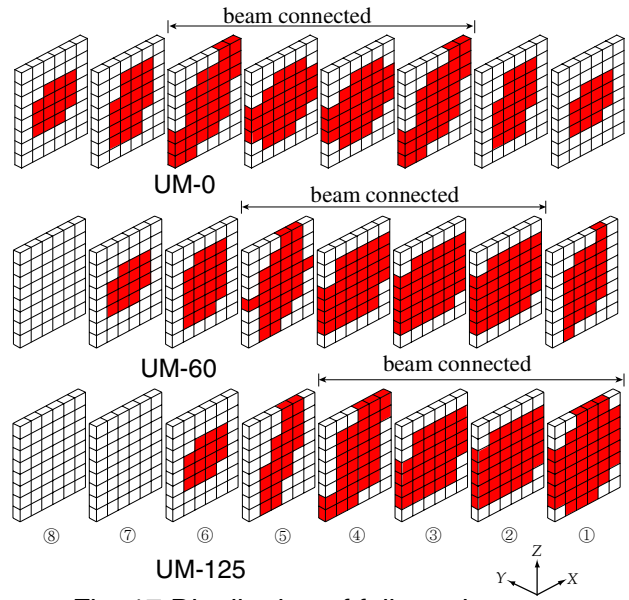


Fig. 17 Distribution of failure elements (at maximum strength)

## CONCLUSIONS

The seismic performance of eccentric interior beam-column connections was investigated experimentally and analytically. The experimental work was carried out using four specimens that were given constant vertical force and cyclic horizontal loading. Then, an analytical study on the specimens was carried out using three-dimensional FEM. Experimental and analytical results revealed the following:

- 1) Comparison of the observed strength between specimens that failed in joint shear indicates that, as the eccentric distance increases, the joint shear strength decreases. This tendency was observed in the experiment as well as the analysis.
- 2) The calculation of joint shear strength using the joint effective width prescribed in the AIJ standard underestimates the experimental results. The degree of underestimation depends on the eccentric distance.
- 3) The joint shear strength calculated by the AIJ equation using the modified effective joint width, which is defined by taking the effectiveness of the joint concrete into consideration, showed the good agreement with the experimental results.

4) The finite element analysis showed that the eccentric distribution of the compressive and shear stresses in the eccentric joint concrete elements caused the local failure of the concrete, whereas there was uniform distribution in the concentric joint. However, the strength decreased more gradually in the eccentric joint than in the concentric joint, because the concrete elements located on the offset side became effective resistance after the ultimate stage.

## ACKNOWLEDGMENT

This work was supported by a Grant-in-Aid for Scientific Research (C), No. 13650612, from Japan Society for the Promotion of Science (JSPS).

## REFERENCES

1. Architectural Institute of Japan "AIJ Standard for Structural Calculation of Reinforced Concrete Structures - Based on Allowable Stress Concept", (Japanese), 1999
2. Architectural Institute of Japan "Recommendation to RC Structural Design after Hanshin-Awaji Earthquake Disaster - Cause of particularly damaged and corresponding RC structural design details", (Japanese), 1999
3. Joh O., Goto Y. and Shibata T. "Behavior of Reinforced Concrete Beam-Column Joints with Eccentricity", Design of Beam-Column Joints for Seismic Resistance, SP-123, American Concrete Institute, pp.317-357, 1999
4. ACI-ASCE Committee 352 "Recommendations for Design Beam-Column Connections in Monolithic Reinforced Concrete Structures (ACI 352R-02)", American Concrete Institute, Farmington Hills, 2002
5. Architectural Institute of Japan "Design Guidelines for Earthquake Resistant Reinforced Concrete Buildings Based on Inelastic Displacement Concept", (Japanese), 1999
6. Meinheit D. F. and Jirsa J. O. "Shear Strength of R/C Beam-Column Connections", ASCE, Journal of the Structural Division, Vol. 107, No. ST11, pp.2227-2244, 1981
7. CEB "CEB-FIP Model Code1990 Design Code", Thomas Telford Service Ltd, 1993
8. W. F. Chen "Plasticity of Reinforced Concrete" MacGraw-Hill International Company, 1982
9. Nakamura H. and Higai T. "Compressive fracture energy and fracture zone length of concrete", Seminar on post-peak behavior of RC structures subjected to seismic loads, JCI-C51E, Vol.2, pp.259-272, 1999
10. TNO Building and Construction Research "DIANA User's Manual Non-linear Analysis, Release 7"
11. Vecchio F. J. and Collins M. P. "The Modified Compression-Field Theory for Reinforced Concrete Elements Subjected to Shear", ACI Structural Journal, Vol.83, No.2, pp.219-231, 1986
12. Morita S. et al. "Basic Experiments and Development of Analytical Models to Improve Accuracy of FEM Analysis of RC Structures", (Japanese) Grant-in-Aid for Scientific Research (A), Japan Ministry of Education, 1989